ARTICLE

Structure and dynamics of triplet-exciton pairs generated from singlet fission studied via magnetic field effects

Masanobu Wakasa[1], Tomoaki Yago [1], Yoriko Sonoda [2] & Ryuzi Katoh[3]

Singlet fission is the conversion of a singlet exciton to a pair of triplet excitons followed by a diffusion process to form two free triplet excitons. The quantum yield of singlet fission per photon can exceed 100%. Singlet fission is thus an attractive way to enhance solar-cell performance. However, singlet fission events are not well characterized. In particular, the structure and diffusion pathways of triplet-exciton pairs, which strongly affect the efficiency of the singlet fission event, are unclear. Here we study the magnetic field effects (MFEs) on the singlet fission of diphenylhexatriene (DPH) and fluorinated DPHs crystals. Their fluorescence intensities show clear MFEs and the shape of the MFE curve depends on the crystal structure. Analysis of MFEs with the stochastic Liouville equation reproduces the MFE curve well. This use of MFEs allows one to determine the structure and diffusion pathways of triplet-exciton pairs, and to predict the efficiency of singlet fission events.

[1] Department of Chemistry, Graduate School of Science and Engineering, Saitama University, 255 Shimo-ohkubo, Sakura-ku, Saitama 338-8570, Japan.
[2] Electronics and Photonics Research Institute, National Institute of Advanced Industrial Science and Technology, Tsukuba, Ibaraki 305-8565, Japan.
[3] Department of Chemical Biology and Applied Chemistry, College of Engineering, Nihon University, Koriyama, Fukushima 963-8642, Japan. Correspondence and requests for materials should be addressed to M.W. (email: mwakasa@chem.saitama-u.ac.jp) or to T.Y. (email: yago@chem.saitama-u.ac.jp)

Singlet fission (SF) is a process by which a singlet exciton (S_1) on a molecule splits into two triplet excitons located on different molecules[1,2]. As shown in Fig. 1, triplet excitons are derived from a correlated triplet-exciton pair (TP). Diffusion of the triplet excitons leads to transformation of the correlated TP into a separated TP and finally yields two free triplet excitons ($2T_1$)[3,4]. The reverse process is triplet fusion (TF), which generates a S_1 from $2T_1$.

The fact that two triplet excitons can each form an electron makes it possible for the quantum yield per photon to exceed 100%[5]. The first generated TP is in a pure singlet state $^1(T_1T_1)$ composed of unpaired electron spins in the TP[3,4,6]. Singlet fission is therefore a spin-allowed process and the generation of triplet excitons occurs rapidly (in some case, on a sub-100 fs timescale) and efficiently[7,8].

Since 2000, interest in singlet fission has been greatly stimulated by the possibility that it might be used to increase the maximum efficiency of solar cells[9] to more than 40%, greater than the value of Shockley–Queisser limit (32%)[10] for single-junction devices. Extensive experimental and theoretical studies of this possibility have been carried out[5,11–29]. As the efficiency of correlated TP generation and the process of fast diffusion of TPs to form free triplet excitons affect the overall efficiency of singlet fission, the characterization of TPs, especially their structure and diffusion pathways, is critical to optimizing singlet fission events. However, this characterization is a difficult task, because the relevant processes—diffusion of a triplet exciton, triple fusion, and the spin dynamics of TP—are complicated. Covalently linked dimers in which triplet excitons are fixed have recently been employed to clarify the structure–function relationship in singlet fission[28–36]. However, details of the structure and diffusion pathways of TPs are still unclear.

In a TP, spin states and spin dynamics are influenced by magnetic fields[1–4,37,38]. In the case of a correlated TP in which there was a distinct exchange interaction, we recently reported that singlet fission from an organic crystal of 1,6-diphenyl-1,3,5-hexatriene (DPH) showed clear magnetic field effects (MFEs) at magnetic field strengths of 0–5 T[38]. These MFEs on the fluorescence of DPH could be explained by the level crossing of correlated TP. We successfully determined the structure of correlated TP in the DPH crystal by analyzing the angular dependence of MFE[37]. Thus, the measurement of MFEs appears to be one of the most powerful methods for investigating singlet fission events in organic materials[1–4].

In the case of a separated TP, the exchange interaction is negligibly small, because the distance between the two triplet excitons is too large. Figure 2 shows a schematic representation of the spin dynamics in TPs generated by singlet fission. In the absence of a magnetic field, some of the initial singlet TPs are converted to quintet and triplet TPs by spin relaxation and coherent spin state mixing induced by dipole–dipole coupling in a triplet exciton (black arrows). Coherent spin conversions caused by dipole–dipole coupling are not allowed between the singlet and triplet directly. However, a singlet TP can be converted to a triplet TP via a quintet if the lifetime of the separated TPs is long enough. As the magnetic field also connects the spin states (blue arrows), the population conversion between the singlet and other spin states of the TP can be accelerated or decelerated by the field. The population of the singlet TP is different in the presence and absence of a magnetic field. As the spin state selective triplet fusion from the singlet TP to the singlet exciton projects the population of the singlet TP onto the population of the singlet exciton, the MFEs on the intensity of fluorescence become apparent. Therefore, MFEs on the fluorescence of organic solids contain much information about the singlet fission events, such as

the singlet fission and triplet fusion rates, diffusion of triplet exciton, and spin dynamics.

Typical MFEs on fluorescence for singlet fission materials consist of (1) a decrease in fluorescence intensity in magnetic fields with strengths weaker than or comparable to that of dipole–dipole coupling and (2) an increase in fluorescence intensity in stronger magnetic fields[3,4]. In the absence of a magnetic field, the spin states in separated TPs are defined based on the dipole–dipole coupling in a triplet exciton. In the presence of an external magnetic field, the spin states in TPs are also affected by the magnetic field. When a weak magnetic field is applied to the TPs, coherent spin-state mixing is enhanced and the population of the singlet state is efficiently transferred to other spin states of the TPs. As a result, the fluorescence intensity decreases in the presence of weak magnetic fields. When a strong magnetic field is applied, the spin states are energetically separated by the Zeeman splitting. The population conversion from the singlet to other spin states is decelerated, the result being an increase of the fluorescence intensity. These characteristics of MFEs depend on the magnitude of the dipole–dipole coupling, which is highly anisotropic. Thus, the MFE in low magnetic fields of < 0.15 T is also anisotropic and is sensitive to the structure of the separated TPs.

Here we study MFEs on the singlet fission of DPH and fluorinated DPH crystals at magnetic field strengths < 0.15 T. Their fluorescence intensities show clear MFEs and the shape of the MFE curve depends on the crystal structure. Analysis of MFEs with the stochastic Liouville equation (SLE) reproduces the MFE curve well together with the structure and diffusion pathways of TPs.

Results

Structure of materials. In this study, the E,E,E isomers of DPH[37,38], 1,6-bis(4-fluorophenyl)-1,3,5-hexatriene (MF)[39], 1,6-bis(2,4-difluorophenyl)-1,3,5-hexatriene (DF)[39], and 1,6-bis(2,4,6-trifluorophenyl)-1,3,5-hexatriene (TFL)[39] were used as singlet fission materials. These materials vary in terms of crystal structures (Fig. 3)[40,41]. In DPH and MF crystals, there is a herringbone structure in addition to a slipped parallel stacking structure. The crystals of DF and TFL are characterized by a slipped parallel stacking structure.

Magnetic field effects. The fluorescence of these materials was carefully measured under magnetic fields of < 0.5 T. Figure 4 shows the typical magnetic field dependence of the relative fluorescence intensity, $R(B)$, of the crystals in powder form for DPH, MF, DF, and TFL in a field of 0.15 T. It is apparent in this figure that $R(B)$ decreases and increases with increasing magnetic field strength in the ranges of $0 < B \leq 0.06$ T and 0.06 T $< B$, respectively. Moreover, it is apparent that there is a clear crystal structure dependence of the MFE on the fluorescence. The MFEs observed for DF (green circles) and TFL (yellow circles) exhibited double minima at the magnetic fields of 0.03 and 0.06 T, whereas the MFEs for DPH (red circles) and MF (black circles) showed a single minimum at the magnetic field strength of 0.06 T. The magnitude of MFEs in low magnetic fields also varied between crystal structures.

Analysis by the SLE. To elucidate the origin of the crystal structure dependence of MFEs, TP dynamics in the absence and presence of magnetic fields were simulated with the SLE, which includes one-dimensional diffusion for one of the triplet excitons, the spin Hamiltonian for the TP, singlet fission, and triplet fusion at a correlated TP[37]. Details are described in Supplementary Methods. Moreover, various orientations of triplet excitons in
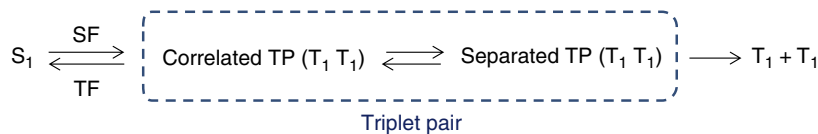
Fig. 1 Schematic representation of singlet fission. A singlet-exciton (S_1) generates two triplet excitons ($2T_1$) through a triplet-exciton pair (TP)
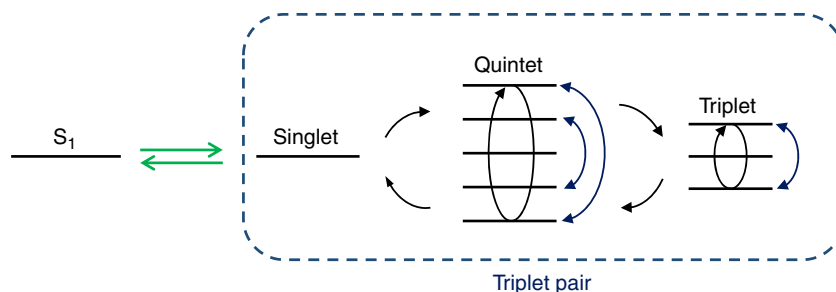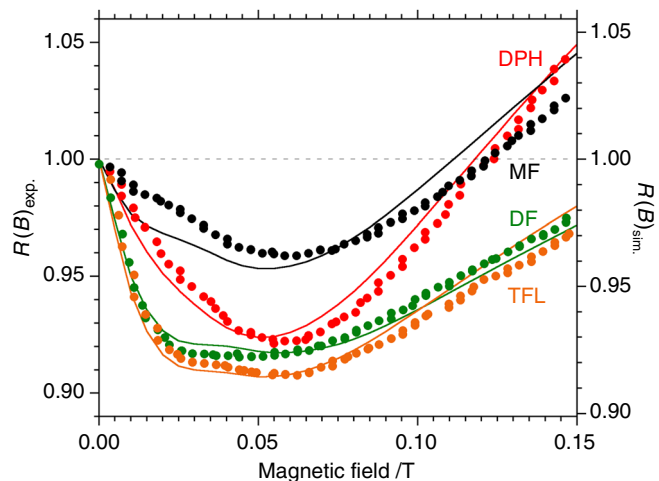

Fig. 2 Schematic representation of spin dynamics in triplet pairs generated by singlet fission. Black arrows show possible population conversions between spin states caused by dipole–dipole coupling in a triplet-exciton and spin relaxation. Blue double-arrows show population conversions between spin states due to the magnetic field. Green arrows indicate spin state selective singlet fission and triplet fusion
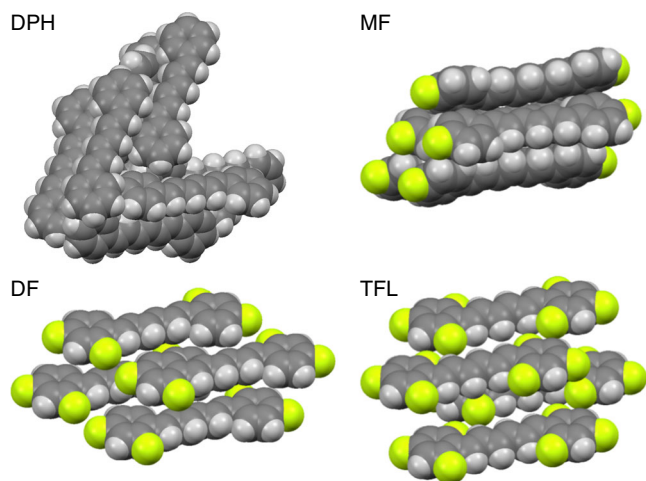
Fig. 3 Crystal structures of DPH and fluorinated DPHs. In the solid state, DPH and MF adopt herringbone structures while DF and TFL adopt slipped parallel stacking structures

Fig. 4 Magnetic field dependence of fluorescence intensity. Observed for the crystals in powder form of DPH (red circles), MF (black circles), DF (green circles), and TFL (yellow circles). Relative fluorescence intensity $R(B)_{\text{exp.}}$ is the fluorescence intensity (F) at each magnetic field strength (B) normalized to the intensity at 0 T ($R(B) = F(B)/F(0)$). Magnetic field dependence of fluorescence intensity simulated by the stochastic Liouville equation for each crystal $R(B)_{\text{sim.}}$ is shown by solid lines with the same colors as the corresponding data

crystals using the dipole–dipole coupling tensor in the spin Hamiltonian were modeled in the present SLE analysis. In DF and TFL crystals, the two triplet excitons in a pair have the same orientation. For DPH and MF crystals, triplet excitons were assumed to diffuse along the herringbone structure, changing their orientations.

The model used in the present study is schematically depicted in Fig. 5. The singlet exciton is initially generated by irradiation. Singlet fission occurs from the singlet exciton with a rate constant k_{SF} to give the correlated triplet pair in the singlet state. This process competes with radiative decay (k_{rad}) of the singlet exciton. In the correlated TP, triplet fusion occurs with a rate constant k_{TF}, regenerating the singlet exciton. Here the singlet exciton is generated only from the correlated TP in the singlet state. Thus, triplet fusion is a spin state selective process. The correlated TP can dissociate to a separated TP with a rate constant k_{dis}. The triplet exciton hops to a neighboring molecule with a rate constant k_{h} in separated TPs. Some of the triplet excitons escape from the pair to give free triplet excitons, which cannot diffuse back to form TPs. In addition to the normal hopping, a shallow

trap site is applied to one of the separated TPs by varying the rate (k_{trap}) of hopping. This modification is necessary to reproduce the fluorescence decay observed in DPH crystal. In our model, the above scheme repeats until the photo-excited singlet state eventually falls into the ground state or the free triplet exciton.

The magnetic field dependence of the fluorescence intensity simulated with the SLE for each crystal is shown in Fig. 4. In the present SLE analysis, the magnitude and curvature of MFEs at low magnetic field strengths were affected by the kinetic parameters associated with the TPs, including the singlet fission rate (k_{SF}), the dissociation rate (k_{dis}) of the correlated TP, the hopping rate (k_{h}) of the triplet exciton, and the triplet fusion rate (k_{TF}) of the correlated TP. The obtained parameters from the best fitted data are listed in Table 1 and Supplementary Table 1, including the quantum yields of total singlet fission event ($\Phi_{\text{SF event}}$).
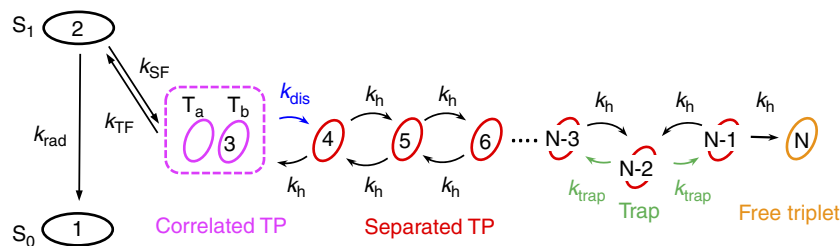
Fig. 5 Model used in the present SLE analysis. Singlet fission to a correlated triplet pair (k_{SF}), radiative decay from the singlet exciton(k_{rad}), dissociation of the correlated triplet pair (k_{dis}), triplet fusion in the correlated triplet pair (k_{TF}), and hopping of triplet excitons in one dimension (k_h) modified by a shallow trap site (k_{trap}). The number for each site is also indicated

Table 1 Obtained parameters from the SLE analysis

Compound	k_{dis}/s^{-1}	k_h/s^{-1}	k_{TF}/s^{-1}	$\Phi_{SF\ event}$
DPH	3.3×10^{10}	8.0×10^{9}	3.0×10^{10}	1.78
MF	6.0×10^{10}	1.0×10^{10}	2.0×10^{10}	1.84
DF	5.0×10^{10}	1.1×10^{11}	4.7×10^{9}	1.86
TFL	4.0×10^{10}	1.0×10^{11}	5.5×10^{9}	1.84

Dissociation rate (k_{dis}) of the correlated triplet pair, hopping rate (k_h) of the triplet exciton, triplet fusion rate (k_{TF}) of the correlated triplet pair, and quantum yield of total singlet fission event ($\Phi_{SF\ event}$)

In the present analyses of DPH, MF, DF, and TFL, the same values of singlet fission rate k_{SF} (5.0×10^9 s^{-1}) were used, because the decay rates of the fluorescence observed in the time range of 0–1 ns were nearly the same (ca. 200 ps) for all compounds[37,39]. In contrast, k_{dis}, k_h, and k_{TF} values differed for compounds. In the cases of DF and TFL, k_h values were much larger than k_{TF}. Moreover, k_{TF} values were smaller for DF and TFL than for DPH and MF.

As described in the Introduction, the diffusion of triplet excitons characterized by rate constants k_{dis} and k_h competes with triplet fusion characterized by rate constant k_{TF}. As the k_{SF} values are nearly the same (5.0×10^9 s^{-1}) in the present reactions of DPH, MF, DF, and TFL, singlet fission should occur efficiently if k_{TF} is relatively small and k_h and k_{dis} are relatively large. As shown in Table 1, the rate constants of k_{dis} and k_h for DF and TFL were much larger than k_{TF}; thus, the singlet fission in DF and TFL is expected to occur efficiently compared with that in DPH and MF. Indeed, the values of $\Phi_{SF\ event}$ estimated from the SLE analysis of DF and TFL are slightly larger than that of DPH. On the other hand, the observed fluorescence quantum yields for DPH, MF, DF, and TFL were nearly the same, 0.010–0.013[39]. This implies that fluorescence quantum yields are not the direct indicators of the efficiency of singlet fission events; however, MFEs can be used to predict the efficiency.

Triplet-exciton diffusion pathways. We will discuss the diffusion pathways of the triplet exciton in the crystal of DPH in detail. The triplet exciton can take several diffusion pathways in the DPH crystal used in this study. To implement the SLE, as shown in Fig. 6, we simplified and classified the triplet-exciton diffusion pathways into (1) the diffusion along the slipped parallel stacking structure, (2) the diffusion with the tilted positions **1** and **2**, and (3) the zigzag diffusions **1** and **2**. On the first step of the diffusion with tilted positions, the tilt occurs only once, in the step from the singlet exciton to the spin correlated pair. Further hopping occurs in a parallel manner. In the zigzag diffusion, the triplet exciton changes its orientation during diffusion and the two triplet excitons in a separated pair alternately take the same and different orientations during diffusion.
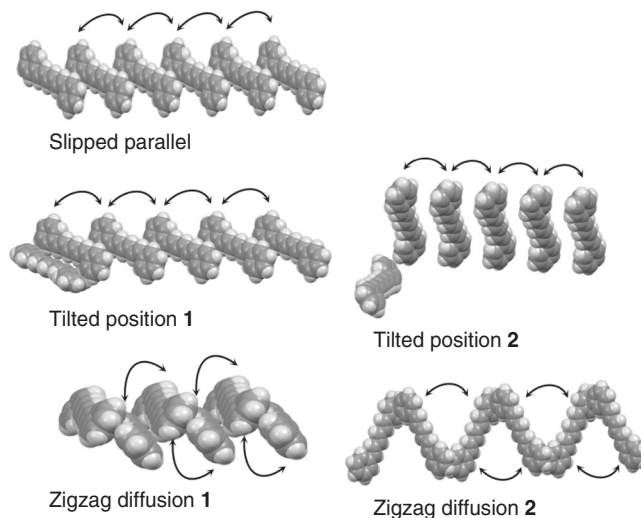
Fig. 6 Diffusion pathways used in the present SLE simulations of the crystals in powder form of DPH. Diffusion along the slipped parallel stacking structure, diffusion with tilted positions **1** and **2**, and zigzag diffusions **1** and **2**

Figure 7 shows the simulated magnetic field dependence of the fluorescence intensity $R(B)_{sim.}$ with various diffusion pathways for the triplet exciton in DPH. When the slipped parallel structure was employed, $R(B)_{sim.}$ exhibited double minima, although DF and TF have such magnetic field dependence of double minima. This result calculated with the slipped parallel structure was different from the observed MFE on $R(B)_{exp.}$ of DPH crystal. If the diffusion with tilted position was assumed, the SLE simulations underestimated or overestimated the decrease in the fluorescence intensity in low magnetic fields. The SLE simulations with zigzag diffusions were the most consistent with the observed MFE for DPH crystal. The red solid line in Fig. 4 was obtained using the weighted average of the MFE data calculated with the zigzag diffusions **1** and **2** with the weighting ratio of 0.65 : 0.35. The SLE analysis suggests that most of the triplet excitons generated in DPH crystal diffuse along the herringbone structure with a mixture of zigzag diffusions **1** and **2**, and those in DF and TFL crystals diffuse along the slipped parallel stacking structure. Consideration of the crystal structure of MF suggests that the triplet excitons can diffuse with zigzag diffusion **1** together with the other diffusion pathways. In the preset analysis shown in Fig. 4, the simulated results for MF were obtained by only using zigzag diffusion **1**. Detailed SLE analysis for the crystal of MF is now in progress.

The simulated results obtained from these analyses are in good agreement with the experimentally observed MFEs. The double minima observed with DF and TFL crystals, in particular, are
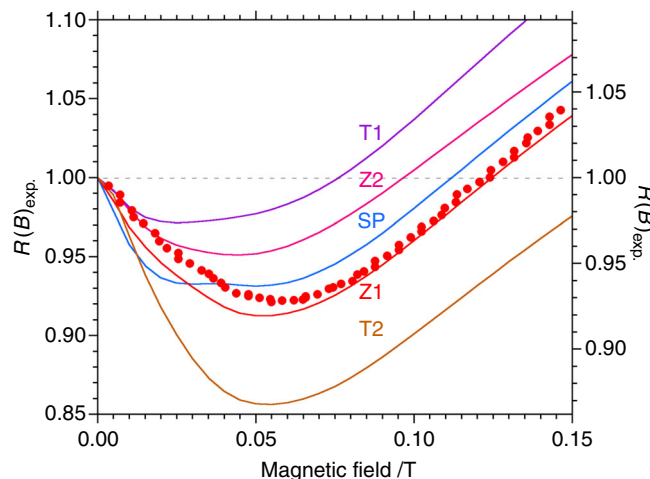
Fig. 7 Magnetic field dependence of fluorescence intensity $R(B)_{sim.}$ calculated with the SLE for the crystals in powder form of DPH. The SLE calculations were performed with diffusion along the slipped parallel stacking structure SP (blue solid line), diffusion with tilted positions T1 (purple solid line) and T2 (brown solid line), and zigzag diffusions Z1 (red solid line) and Z2 (pink solid line). The experimental results $R(B)_{exp.}$ are indicated with filled red circles

nicely reproduced using the slipped parallel stacking structure in the simulations. The SLE analysis provides the following insights about the MFE in low magnetic fields. (1) The double minima in low magnetic fields are caused by an overlap of the typical low-field MFE[42,43] and the MFE due to the level crossing between spin states at the magnetic field strength where the Zeeman splitting matches the dipole–dipole coupling. (2) The typical low-field MFE decreases the fluorescence intensity by accelerating transitions from the singlet and other spin states in TPs. (3) The level crossing decelerates the state transitions and thus increases the fluorescence intensity. In DF and TFL crystals, the magnetic field at which the level crossing between spin states occurs was calculated to be 0.04 ± 0.01 T. The fluorescence intensity was thus increased at 0.04 T, the result being formation of the double minima at 0.03 and 0.06 T.

In the simulations of DF and TFL with the slipped parallel stacking structures, the double minima survived in the curves shown in Fig. 4, whereas the double minima were diminished in DPH and MF with the herringbone structures. This difference should be caused by the different spin state interactions between the slipped parallel stacking and herringbone structures at low magnetic fields. The singlet state of TP can interact with two spin states in the slipped parallel structure, whereas in the herringbone structure the singlet state can interact with eight spin states. The spin population can thus be distributed among three spin states in the slipped parallel stacking structure, whereas it can be distributed among nine spin states in the herringbone structure. In the cases of slipped parallel stacking, the singlet character is concentrated (ca. 48%) on one of the spin eigenstates as shown in Supplementary Figure 1. On the other hand, the concentration of the singlet character for each spin eigenstates for herringbone structure does not exceed 30%. Thus, the effect of the level crossing is smaller in the herringbone structure than in the slipped parallel stacking structure. The effect of level crossing on the MFE is thus most apparent for the slipped parallel stacking structure. Based on this analysis, we can safely conclude that the triplet excitons diffuse along the herringbone structures in DPH and MF crystals. The SLE analysis revealed that the shape of the MFE at low magnetic field strengths is sensitive to the orientation of the triplet excitons.

We successfully characterized the structure of the separated TP and the diffusion pathway of the triplet exciton by using MFEs on the fluorescence of DPH and fluorinated DPHs. The structure and diffusion pathway affect the efficiency of singlet fission events. The present methods based on MFEs observed with a conventional magnetic field (< 0.15 T) are useful for finding and designing efficient singlet fission materials.

Methods

Chemical synthesis and characterisation. DPH was purchased from Wako (Apollo Scientific, OR6793) and used as received. The purity of DPH was high and we could obtain small but high quality crystals. The phase of DPH crystals from Wako was determined to be orthorhombic by single crystal X-ray diffraction measurements. The syntheses and characterizations of fluorinated DPHs crystals of MF, DF, and 1,6-bis(2,4,6-trifluorophenyl)-1,3,5-hexatriene (TFL) are described elsewhere[40,41].

Steady-state fluorescence measurements. Steady-state fluorescence measurements in the absence and presence of magnetic fields ($0 \leq B \leq 0.5$ T) were carried out using a super conducting magnet (TOSHIBA, TM-5HSP). The powder form DPH, MF, DF, and TFL crystals were placed in a water jacketed glass container (Id. 20 mm, L. 200 mm) designed for the measurement of fluorescence in the magnet. The temperature for the measurements was maintained at 293 ± 0.5 K by circulating water with a cooling thermo-pump (IWAKI, CTS-134A). The inside of the glass container was filled with Ar gas (40 ml min^{-1}) during the measurements to avoid sample damage by air. A LED lamp ($\lambda = 365$ nm, Tholabs, M365L2) was used as an excitation light source. The excitation light was guided to the sample in the magnet using a quartz optical fiber. The fluorescence from the sample was guided using another optical fiber and detected by a photosensor module (Hamamatsu, H7422-01) after passing a band-pass filter (Tholabs, FB460-10) and a monochromator (Nikon, P250) set at a wavelength of 460 nm. The current from the photosensor was amplified by a low noise current amplifier (Femto, DLPCA-200) and was digitized by a digital multimeter (Agilent, 34401A).

References

1. Smith, M. B. & Michl, J. Singlet fission. *Chem. Rev.* **110**, 6891–6936 (2010).
2. Smith, M. B. & Michl, J. Recent advances in singlet fission. *Annu. Rev. Phys. Chem.* **64**, 361–386 (2013).
3. Johnson, R. C. & Merrifield, R. E. Effects of magnetic fields on the mutal annihilation of triplet excitons in anthracene crystals. *Phys. Rev. B* **1**, 896–902 (1970).
4. Merrifield, R. E. Magnetic effects on triplet exciton interactions. *Pure Appl. Chem.* **27**, 481–498 (1971).
5. Congreve, D. N. et al. External quantum efficiency above 100 % in a singlet-exciton-fission-based organic photovoltaic cell. *Science* **340**, 334–337 (2013).
6. Merrifield, R. E., Avakian, P. & Groff, R. P. Fission of singlet excitons into pairs of triplet excitones in tetracene crystals. *Chem. Phys. Lett.* **3**, 155–157 (1969).
7. W.-L. Chan, M. Ligges, A. Jailaubekov, L. Kaake, L. Miaja-Avila, X.- Y. Zhu, (2011) Observing the multiexciton state in singlet fission and ensuing ultrafast multielectron transfer. Science 334, 1541–1545 (2011).
8. Wilson, M. W. B. et al. Ultrafast dynamics of exciton fission in polycrystalline pentacene. *J. Am. Chem. Soc.* **133**, 11830–11833 (2012).
9. Hanna, M. C. & Nozik, A. J. Solar conversion efficiency of photovoltaic and photoelectrolysis cells with carrier multiplication absorbers. *J. Appl. Phys.* **100**, 074510 (2006).
10. Shockley, W. & Queisser, H. J. Detailed balance limit of efficiency of p-n junction solar cells. *J. Appl. Phys.* **32**, 510–519 (1961).
11. Zimmerman, P. M., Zhang, Z. & Musgrave, C. B. Singlet fission in pentacene through multi-exciton quantum states. *Nat. Chem.* **2**, 648–652 (2010).
12. Chan, W.-L., Ligges, M. & Zhu, X. Y. The energy barrier in singlet fission can be overcome through coherent coupling and entropic gain. *Nat. Chem.* **4**, 840–845 (2012).
13. Walker, B. J., Musser, A. J., Beljonne, D. & Friend, R. H. Singlet exciton fission in solution. *Nat. Chem.* **5**, 1019–1024 (2013).
14. Yost, S. R. et al. A transferable model for singlet-fission kinetics. *Nat. Chem.* **6**, 492–497 (2014).

15. Wan, Y. et al. Cooperative singlet and triplet exciton transport in tetracene crystals visualized by ultrafast microscopy. *Nat. Chem.* **7**, 785–792 (2015).

16. Stern, H. L. et al. Identification of a triplet pair intermediate in singlet exciton fission in solution. *Proc. Natl Acad. Sci. USA* **112**, 7656–7661 (2015).

17. Bakulin, A. A. et al. Real-time observation of multiexcitonic state in ultrafast singlet fission using coherent 2D electronic spectroscopy. *Nat. Chem.* **8**, 16–23 (2016).

18. Margulies, E. et al. Enabling singlet fission by controlling intramolecular charge transfer in π-stacked covalent terrylenediimide dimers. *Nat. Chem.* **8**, 1120–1125 (2016).

19. Monahan, N. et al. Dynamics of the triplet-pair state reveals the likely coexistence of coherent and incoherent singlet fission in crystalline hexacene. *Nat. Chem.* **9**, 341–346 (2016).

20. Mauck, C. M. et al. Singlet fission via an excimer-like intermediate in 3,6-bis (thiophen-2-yl)diketopyrrolopyrrole derivatives. *J. Am. Chem. Soc.* **138**, 11749–11761 (2016).

21. Pensack, R. D. et al. Observation of two triplet-pair intermediates in singlet exciton fission. *J. Phys. Chem. Lett.* **7**, 2370–2375 (2016).

22. Miyata, K. et al. Coherent singlet fission activated by symmetry breaking. *Nat. Chem.* **9**, 983–989 (2016).

23. Yong, C. K. et al. The entangled triplet pair state in acene and heteroacene materials. *Nat. Commun.* **8**, 15953 (2017).

24. Piland, G. B., Burdett, J. J., Kurunthu, D. & Bardeen, C. J. Magnetic field effects on singlet fission and fluorescence decay dynamics in amorphous rubrene. *J. Phys. Chem. C* **117**, 1224–1236 (2013).

25. Burdett, J. J., Piland, G. B. & Bardeen, C. J. Magnetic field effects and the role of spin states in singlet fission. *Chem. Phys. Lett.* **585**, 1–10 (2013).

26. Dillon, R. J., Piland, G. B. & Bardeen, C. J. Different rates of singlet fission in monoclinic versus orthorhombic crystal forms of diphenylhexatriene. *J. Am. Chem. Soc.* **135**, 17278–17281 (2013).

27. Piland, G. B., Burdett, J. J., Dillon, R. J. & Bardeen, C. J. Singlet fission: from coherences to kinetics. *J. Phys. Chem. Lett.* **5**, 2312–2319 (2014).

28. Tarasov, V. V., Zoriniants, G. E., Shushin, A. I. & Triebel, M. M. The role of spin-lattice relaxation in magnetic field effects on the luminescence of amorphous and polycrystalline rubrene films. *Chem. Phys. Lett.* **267**, 58–64 (1997).

29. Zirzlmeier, J. et al. Singlet fission in pentacene dimers. *Proc. Natl Acad. Sci. USA* **112**, 5325–5330 (2015).

30. Sanders, S. N. et al. Quantitative intramolecular singlet fission in bipentacenes. *J. Am. Chem. Soc.* **137**, 8965–8972 (2015).

31. Lukman, S. et al. Tuneable singlet exciton fission and triplet-triplet annihilation in an orthogonal pentacene dimer. *Adv. Funct. Mater.* **25**, 5452–5461 (2015).

32. Sanders, S. N. et al. Intramolecular singlet fission in oligoacene heterodimers. *Angew. Chem. Int. Ed. Engl.* 55, (3373–3377 (2016).

33. Cook, J. D., Carey, T. J. & Damrauer, N. H. Solution-phase singlet fission in a structurally well-defined norbornyl-bridged tetracene dimer. *J. Phys. Chem. A.* **120**, 4473–4481 (2016).

34. Sakuma, T. et al. Long-lived triplet excited states of bent-shaped pentacene dimers by intramolecular singlet fission. *J. Phys. Chem. A.* **120**, 1867–1875 (2016).

35. Lukman, S. et al. Tuning the role of charge-transfer states in intramolecular singlet exciton fission through side-group engineering. *Nat. Commun.* **7**, 13622 (2016).

36. Korovina, N. V. et al. Singlet fission in a covalently linked cofacial alkynyltetracene dimer. *J. Am. Chem. Soc.* **138**, 617–627 (2016).

37. Yago, T., Ishikawa, K., Katoh, R. & Wakasa, M. Magnetic field effects on triplet pair generated by singlet fission in an organic crystal: application of radical pair model to triplet pair. *J. Phys. Chem. C* **120**, 27858–27870 (2016).

38. Wakasa, M. et al. What can be learned from magnetic field effects on singlet fission: Role of exchange interaction in excited triplet pairs. *J. Phys. Chem. C* **119**, 25840–25844 (2015).

39. Katoh, R. et al. Singlet fission in fluorinated diphenylhexatrienes. *J. Phys. Chem. C* **121**, 25666–25671 (2017).

40. Sonoda, Y., Goto, M., Tsuzuki, S. & Tamaoki, N. Fluorinated diphenylpolyenes: crystal structures and emission properties. *J. Phys. Chem. A* **111**, 13441–13451 (2007).

41. Sonoda, Y. et al. Halogenated (F, Cl, Br, or I) diphenylhexatrienes: crystal structures, fluorescence spectroscopic properties, and quantum chemical calculations. *Cryst. Growth Des.* **16**, 4060–4071 (2016).

42. Timmel, C. R., Till, U., Brocklehurst, B., McLauchlan, K. A. & Hore, P. J. Effects of weak magnetic fields on free radical recombination reactions. *Mol. Phys.* **95**, 71–89 (1998).

43. Woodward, J. R. et al. Radio frequency magnetic field effects on electron-hole recombination. *Phys. Rev. Lett.* **87**, 077602–077604 (2001).

Acknowledgements

Author contributions

M.W. conceived the project. M.W. and R.K. carried out the experiments. T.Y. analyzed the data. Y.S. provided the materials. All authors discussed the results. M.W. and T.Y. wrote the manuscript with input from all authors.

Additional information

Supplementary Information accompanies this paper at https://doi.org/10.1038/s42004-018-0008-0.

Competing interests: The authors declare no competing interests.

Reprints and permission information is available online at http://npg.nature.com/reprintsandpermissions/

Publisher's note: Springer Nature remains neutral with regard to jurisdictional claims in published maps and institutional affiliations.